

# Towards Learning Neural Representations from Shadows

Kushagra Tiwary <sup>\*†</sup>, Tzofi Klinghoffer <sup>\*</sup>, and Ramesh Raskar

Massachusetts Institute of Technology  
{ktiwary, tzofi, raskar}@mit.edu

**Abstract.** We present a method that learns neural scene representations from *only* shadows present in the scene. While traditional shape-from-shadow (SfS) algorithms reconstruct geometry from shadows, they assume a fixed scanning setup and fail to generalize to complex scenes. Neural rendering algorithms, on the other hand, rely on photometric consistency between RGB images but largely ignore physical cues such as shadows, which have been shown to provide valuable information about the scene. We observe that shadows are a powerful cue that can constrain neural scene representations to *learn* SfS, and even outperform NeRF to reconstruct otherwise hidden geometry. We propose a graphics-inspired differentiable approach to render accurate shadows with volumetric rendering, predicting a shadow map that can be compared to the ground truth shadow. Even with just binary shadow maps, we show that neural rendering can localize the object and estimate coarse geometry. Our approach reveals that sparse cues in images can be used to estimate geometry using differentiable volumetric rendering. Moreover, our framework is highly generalizable and can work alongside existing 3D reconstruction techniques that otherwise only use photometric consistency. Our code is made available in our supplementary materials.

**Keywords:** Scene Representations, Differentiable Rendering, 3D Scene Reconstruction, Shape-from-Shadows, Volume Rendering

## 1 Introduction

Recovering 3D geometry from 2D images remains an extremely important, yet unsolved, problem in computer vision and inverse graphics. Considerable progress has been made in the field when assumptions are made, such as bounded scenes, diffuse surfaces, and specific materials. However, reconstruction algorithms still remain largely susceptible to real world effects, such as specularities, shadows, and occlusions [34]. This susceptibility is largely due to the variation in different materials, textures and a non-unique mapping from 3D geometries to 2D images. Even though these effects cause issues for many methods, they also provide valuable information about the scene and geometry of the object. For example, cues like self-shadows provide vital information about an object’s concavities, while shadows cast on the ground plane provide information about its geometry. Moreover,

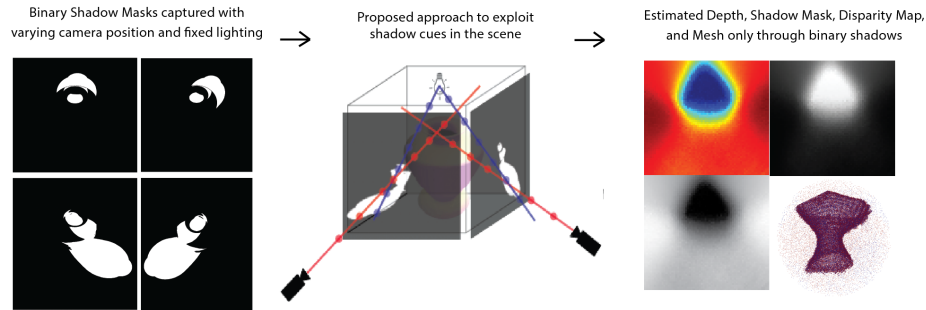


**Fig. 1. Exploiting physical cues in neural rendering.** Our approach takes sparse binary shadow masks captured with varying camera positions under fixed lighting and uses our proposed differentiable shadow rendering model to estimate shadow maps, thereby learning neural scene representations. We can visualize the learned implicit representations by rendering estimated depth maps and estimated shadow maps from novel views. We also run marching cubes [14] on our learned representations to get explicit meshes for a quantitative analysis.

shadows are independent of textures and surface reflectance models and are a strong cue in overhead imagery where vertical surfaces, like facades, are sampled poorly, whereas oblique lighting can expose this geometry. Exploiting, instead of ignoring these cues, can make algorithms robust and the fundamental problem of 3D reconstruction less ill-posed.

Previous works in recovering 3D shape of objects by exploiting physical cues has relied on constructing an inverse model to explicitly handle and exploit cues such as shadows, shading, motion, or polarization [2] [40] [39]. These approaches are physically anchored as they use properties of light or surface reflectance models to exploit cues and only need up to a single image to reconstruct simple objects. Albeit successful under strict assumptions about lighting, camera and the object, these models typically cannot handle complex scenes and do not translate well into real-world scenarios as creating inverse models to capture complex physical phenomenon soon becomes intractable and hard to optimize over.

To combat the problem of real world variability, modern methods such as [30] [16] [21] [27] [36] [12] have largely been data-driven by directly learning 3D representations on real world scenes based on photometric consistency. Such methods employ an *analysis-by-synthesis* approach to solve the problem by using machine learning to search the space of possible 3D geometries and an inverse model to synthesize the scene based on the input predicted geometries. These approaches typically only optimize the photometric loss between different camera viewpoints and show success in learning the implicit representation by rendering novel view synthesis. However, because they do not explicitly handle these physical cues in their forward model, they fail in scenarios with complex lighting [28], specularity [38], or reflections [6].

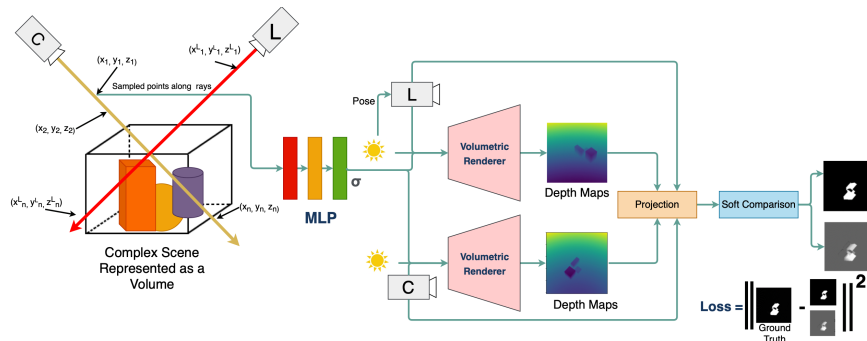


**Fig. 2. Overview of the proposed pipeline** We train a neural network to predict opacity at points along the camera and light rays. The opacities are used by the volumetric renderer to output the ray-termination distance which we use to estimate the *z-buffer* from the camera and the light perspective, the latter also known as the shadow map. The estimated *z-buffer* is fed into a **Projection** step that projects the camera pixels and their associated depths into the light’s reference frame. The shadow map is indexed to obtain the corresponding depth values at these new points. The projected depths and indexed depths go through a **Soft Comparison** step which outputs predicted cast shadows in the scene from the camera’s perspective. A loss is computed on the *predicted* and the *ground-truth* shadow mask.

Motivated by the above observations, we explore what can be learned by exploiting physical cues in a data-driven neural rendering framework. In this paper, we investigate whether the neural rendering framework can learn geometry from physical cues without the assumptions made by the aforementioned methods. We study the use of shadows cast by objects onto themselves and nearby surfaces as the only source of information for 3D reconstruction. While modern approaches for 3D reconstruction ignore such cues, we aim to exploit them. Our unsupervised approach uses *only* shadows to reconstruct the scene by leveraging recent advances in volumetric rendering and machine learning, and therefore proposes a physically anchored data-driven framework to the problem of shape from shadows. Moreover, unlike previous work in shape from shadows, we present a novel method that uses differentiable rendering in the loop to iteratively reconstruct the object based on a loss function instead of iteratively refining the object through explicit carving. Specifically, we use an efficient shadow rendering technique called shadow mapping as the forward model and make it differentiable so that it can be used as an inverse model to iteratively reconstruct the object. Our work also reveals that from limited cues the differentiable volumetric rendering component can *quickly converge to localize and reconstruct a coarse estimate of the object when such cues are explicitly modeled by a forward model*. Our work also suggests that neural rendering can exploit shadows to recover hidden geometry, which otherwise may not be discovered by photometric cues.

## 1.1 Contributions

Our contributions in this paper are the following:

- A framework that directly exploits physical cues like shadows in neural renderers to recover scene geometry.
- A novel technique that integrates volumetric rendering with a graphics-inspired forward model to render shadows in an end-to-end differentiable manner.
- Results showing that our framework can learn coarse scene representations from just shadows masks. We evaluate the learned representations qualitatively and quantitatively against vanilla neural rendering approaches. To the best of our knowledge, we are the first to show that it is possible to learn neural scene representations from binary shadow masks.

## 2 Related Work

**Shape from Shadows.** Shadowgram imaging deals with estimating the shape of an object through a sequence of shadow masks captured with light sources at various locations. These methods typically assume a controlled and fixed object scanning setup [26] [33]. Martin & Aggarwal [15] introduced a volumetric space carving approach to SfS which outputs a visual hull around the object by carving out voxels lying outside the visual cone. Other work takes a more probabilistic approach to the shape-from-silhouettes problem to make the algorithm more robust to errors [9]. However, interpreting shadows as silhouettes means that self-shadows are not handled, thus motivating Savarese et al. [26] to propose a method to “carve” out objects based on self-shadows to create more complete reconstructions.

In contrast, our work takes a differentiable approach to solving the problem through learning. Instead of an explicit carving of voxels we first construct a differentiable forward model that casts shadows based on some geometry. Then, we let the machine learning component predict geometry, which is synthesized by the renderer to cast shadows. Finally, we optimize this setup based on a mean square error between predicted and ground truth shadow masks.

**Neural Rendering** Broadly speaking, a neural rendering framework is composed of a differentiable renderer, which can render the scene based on input parameters and is able to differentiate the scene w.r.t. those input parameters. While there are many formulations of differentiable renderers [20] [13] [10] [8] that can synthesize scenes, state-of-art approaches have shown tremendous success by relying differentiable volumetric rendering [19]. Volumetric rendering approaches can realistically render complex scenes and are gradient-friendly. Thus, typical approaches train a neural network to encode the scene and optimize it for photometric consistency between input 2D images from different viewpoints [16] [27] [17] [18]. Recent methods such as [6] [32] [28] [3] explicitly account for specular, reflections and other such phenomenon, however, the goal of these works are to improve novel view synthesis. Thus, these methods still rely on learning the scene using photometric information.

In contrast, our work deals with 3D reconstruction, not novel view synthesis, and explores what can be learned by relying on shadow cues in the scene. Our

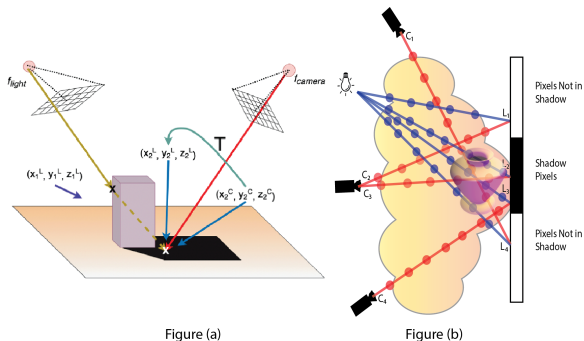


**Fig. 3.** Figure (a): A point  $\mathbf{x} \in \mathbb{R}^3$  in the scene is defined to be in shadow if no direct path exists from the point  $\mathbf{x}$  to the light source which implies that there **must** be an occluding surface between  $\mathbf{x}$  and the light source. We differentially render the scene’s depth from the camera and the light’s perspective at each pixel and then project the camera pixel and its depth into the light’s frame of reference. We then index the light’s depth map, or z-buffer, to get  $z_1^L$ . We note that  $z_1^L$  is less than  $z_2^L$ , i.e. there must be an occluding surface as a ray projected from the light’s perspective terminates early. This implies that this point is in shadow. Figure (b) shows a 2D slice of our approach and represents a volume (cloud) with the shadow mask unraveled. The network learns an opacity per point (dots) via the shadow mapping objective which penalizes predicted geometries that don’t cast perfect ground truth shadows. Through this, the networks learn 3D geometry that is consistent across all shadows maps for all cameras given a particular light source.

framework only operates in the shadow input and output space to infer a 3D representation of the scene. In addition, similar to [25] [37], our work also reveals that differentiable volumetric rendering is a powerful component that can learn the scene by only relying on sparse physical cues. While volumetric approaches rely on a photometric cues, differentiable rasterization [8] [11] has been shown to reconstruct 3D mesh using single low dimensional images of ShapeNet objects [4] by only using silhouettes. However, these methods fail to show success on high dimensional images, while our approach can scale up to higher dimensional images.

**Shadows in Graphics.** Graphics deals with the forward model and shadow mapping [35] is one of the most efficient techniques to render shadows in a scene given the scene’s geometry, camera viewpoint and light position. While differentiability is not important for graphics, we make the shadow mapping framework differentiable to work with modern 3D reconstruction algorithms. We describe the algorithm and our implementation in Section 3.

### 3 Neural Representations From Shadows

Our goal is to recover the scene through shadows cast on the other objects or onto itself. Our method recovers shadows in an image by applying a threshold on that

image thereby making no distinction between types of shadows. We show how we model the shape-from-shadows problem using differentiable rendering and implicit representations in Section 3.1 and our graphics-inspired differentiable forward model in Section 3.2. In Section 3.3, we discuss our additional techniques that we use to enable optimization on binary shadow masks.

### 3.1 Scenes as Neural Shadow Fields

**Implicit Scene Representations.** Similar to Mildenhall *et al.* [16], we represent a continuous scene by parametrizing it using a learnable function  $f_\theta$ . However, our approach does not include any photometric component therefore we represent the scene as 3D function with input  $\mathbf{x} = (x, y, z)$  and a volumetric density  $\sigma$  as output.

$$\gamma(\mathbf{x}) = \left( \sin(2^0 \pi \mathbf{x}), \cos(2^1 \pi \mathbf{x}), \dots, \sin(2^L - 1 \pi \mathbf{x}), \cos(2^L - 1 \pi \mathbf{x}) \right) \quad (1)$$

$$f_\theta : \mathbb{R}^L \rightarrow \mathbb{R}^+; (\gamma(\mathbf{x})) \mapsto (\sigma)$$

We use a positional-encoded 3D point  $\gamma(\mathbf{x}), \{\gamma(\mathbf{x}) \in \mathbb{R}^L, \mathbf{x} \in \mathbb{R}^3\}$  as input which maps to an associated volumetric density  $\sigma \in \mathbb{R}^+$  [16] [29]. In contrast,  $f$  does not encode view dependant color and is independent to viewing direction.

**Volumetric Renderer.** We define a volumetric renderer  $\mathbf{R}_{\text{vol}}$  that takes  $N$  opacities  $\{\sigma\}_{i=1}^N$  at  $N$  discretely sampled points  $\{\mathbf{x}\}_{i=1}^N$  along a ray  $\mathbf{r}$ .

$$\mathbf{R}_{\text{vol}} : [\mathbb{R}^+]_{i=1}^N \rightarrow [\mathbb{R}^+]_{i=1}^N; (\{\sigma\}_{i=1}^N) \mapsto (\mathbf{d}) \quad (2)$$

Since we only have binary shadows as input, we modify the renderer in to output the ray termination distance,  $\mathbf{d}$ , instead of the radiance at that ray.  $\mathbf{R}_{\text{vol}}$  is not a trainable component, but the ray termination distance,  $\mathbf{d}$ , is differentiable w.r.t. the input opacities. The estimated ray-termination distance, range, is computed as follows:

$$\hat{\mathbf{D}}(\mathbf{r}) = \sum_{i=1}^N T_i \alpha_i t_i; \quad T_i = \prod_{j=1}^{i-1} (1 - \alpha_j); \quad \alpha_i = (1 - e^{-\sigma_i \delta_i}) \quad (3)$$

We sample  $\mathbf{r}(t)$  at points  $\{t_0, \dots, t_N\}$  and evaluate the function  $\mathbf{r}(t) = \mathbf{o} + t\mathbf{d}$  to get sampled points  $\{x_0, \dots, x_N\}$  in the scene.  $T_i$  is defined as the cumulative transmittance from  $t_0$  until  $t_i$  and  $\delta_i = t_{i+1} - t_i$  which is the distance between two samples.  $\sigma_i$  is the estimated opacity at point  $i$  by a learned function  $f_\theta$ . Intuitively, the renderer gives us the ray termination distance for each ray shooting through a pixel.

### 3.2 Differentiable Shadow Mapping

We define any point  $\mathbf{x} \in \mathbb{R}^3$  in the scene to be in shadow if no direct path exists from point  $\mathbf{x}$  to the light source  $\mathbf{L}$ . This logic implies that there **must** be

some object or an occluding surface between the point  $\mathbf{x}$  and  $\mathbf{L}$  that occludes the light ray from reaching point  $\mathbf{x}$ . In graphics, shadow mapping [35] uses this observation to construct a forward model to render efficient and accurate shadows in the scene based on known light and camera sources. Our approach makes this efficient shadow rendering forward model differentiable so that it can be used as an inverse model. We then pose the problem of shape from shadows and use our proposed inverse model to estimate the 3D geometry of the scene.

**Estimated z-buffer.** We first evaluate the renderer from the camera’s perspective to get the estimated ray termination distance, or range map,  $\hat{\mathbf{D}}_{cam}$  for all rays coming out of the binary shadow map. However, shadow mapping requires the depth perpendicular to the image plane, i.e along the z axis of the camera’s local coordinate system. This depth is equivalent to a *z-buffer* in graphics and we refer to this value as the *depth* at that pixel. We define a function  $g$  to estimate the *z-buffer*  $\hat{\mathbf{Z}}$  from the range map  $\hat{\mathbf{D}}$ .

$$\hat{\mathbf{z}}_{u,v} = g(\mathbf{d}_{u,v}) = \frac{\mathbf{d}_{u,v}}{\|(u, v, 1) \cdot \mathcal{E}\|_2} \quad (4)$$

The function takes a ray shooting from a pixel  $(u, v)$  and a predicted range,  $\hat{\mathbf{D}}_{cam}^{u,v}$  as input.  $\mathcal{E}$  is the rotational component of the camera’s extrinsic matrix,  $\mathbf{d}_{u,v}$  is the ray termination distance from camera’s focal point, and  $\hat{\mathbf{z}}_{u,v}$  is the depth along the z-axis from the pixel  $(u, v)$ . We also compute the estimated z-buffer from the light’s perspective, which we refer to as the estimated *shadow map*.

**Projection.** With the estimated depths at each pixel from the camera and the light source, we now need to estimate which camera pixels are in shadow given the particular light source. As illustrated in Figure 3, we do this by projecting all pixels and their associated depths visible by the camera into the light’s frame of reference. We then use this projected coordinate to index the shadow map to get the depth to that point from the light’s perspective. We formally write this as follows:

$$\begin{aligned} (U_{cam}^l, V_{cam}^l, \hat{\mathbf{Z}}_{cam}^l) &= (U_{cam}, V_{cam}, \hat{\mathbf{Z}}_{cam}) \cdot P_{light\_from\_cam} \\ \hat{\mathbf{Z}}_{light}^{U_c^l, V_c^l} &= \hat{\mathbf{Z}}_{light} \left[ U_{cam}^l, V_{cam}^l \right] \end{aligned} \quad (5)$$

Here,  $\hat{\mathbf{Z}}_{cam} \in \mathbb{R}^{H \times W}$  is the estimated z-buffer from the camera’s perspective at pixels  $\{U_{cam}, V_{cam}\} \in \mathbb{R}^{H \times W}$ .  $P_{light\_from\_cam}$  is the projection matrix to the light’s reference frame from the camera’s. We denote  $(U_{cam}^l, V_{cam}^l, \hat{\mathbf{Z}}_{cam}^l)$  as the pixels and depth in camera’s frame (subscript) projected into the light’s frame, denoted by the superscript  $l$ . We index the shadow map,  $\hat{\mathbf{Z}}_{light} \in \mathbb{R}^{H \times W}$ , at the projected camera pixels to retrieve the depth of the projected camera pixels from the light source. This is denoted as  $\hat{\mathbf{Z}}_{light}^{U_c^l, V_c^l}$  which is the shadow map indexed at pixel locations  $U_c^l, V_c^l$ . In practice, not all pixels will project within the shadow map’s height and width constraints specified at the start of training. In

graphics, these pixels are usually ignored, however, we clamp all our projections to lie within the height and width bounds to maintain differentiability.

**Soft Comparison.** Once we have the depths to the projected camera pixels and the depths from the light source to those pixels in the same reference frame, we can then compare them to discover if the camera pixel is in shadow. As illustrated by Figure 3, if the depth from the light source to a point is less than the depth from the camera projected into the light’s frame, it means that the light ray must have intersected an object before reaching that point. Thus, that point must be in shadow. Based on this logic, we formulate a soft comparison, which compares different depths to output the predicted binary shadow mask as follows:

$$\begin{aligned}\Delta\hat{Z}_{light} &= \left(\hat{\mathbf{Z}}_{cam}^l - \hat{\mathbf{Z}}_{light}^{U_c^l, V_c^l}\right) \\ \hat{\mathbf{M}}_{binary} &= \mathbf{max}\left(\frac{\Delta\hat{Z}_{light}}{\beta}, \epsilon\right)\end{aligned}\quad (6)$$

We denote  $\hat{\mathbf{M}} \in \mathbb{R}^{H \times W}$  as the output of the entire pipeline: predicted shadow masks. The input to our soft comparison is the projected camera z-buffer into the light’s frame,  $\hat{\mathbf{Z}}_{cam}^l$ , and the shadow map indexed at the projected points  $\hat{\mathbf{Z}}_{light}^{U_c^l, V_c^l}$  from the **Projection** step.  $\beta$  is a scaling hyper-parameter used to enlarge or decrease the difference, and  $\epsilon$  is a threshold. We also formulate a “smoother” version of the predicted shadows:

$$\hat{\mathbf{M}}_{smooth} = \mathbf{S}\left(\mathbf{normalize}(\Delta\hat{Z}_{light}, \mu_{min}, \mu_{max})\right)\quad (7)$$

Here,  $\mu_{min}, \mu_{max}$  are used to control the normalization function and  $\mathbf{S}$  is the sigmoid function.

### 3.3 Optimization

To enable convergence, we smooth the binary ground truth shadow masks  $\mathbf{M}$  to better guide the framework in predicting accurate shadow masks.

**Distance Transform.** Binary images contain limited information for differentiation as the gradient is zero everywhere except for the edges where it is one. To encourage our model to estimate better shadow masks, thereby learning a better 3D model, we use a distance transform on the ground truth shadow masks. Specifically, we scale pixel intensities of a binary shadow mask by their distance to the nearest shadow edge. We modify the weighted distance transform in [24] for our approach. The transformed binary shadow mask,  $w(\mathbf{M}, \sigma) = \mathbf{M}_w$  is computed as follows:

$$w(\mathbf{M}, \sigma) = \mathbf{M} + \left(w_c(\mathbf{M}) + w_0 \cdot \exp\left(-\frac{(d_1(\mathbf{M}) + d_2(\mathbf{M}))^2}{2\sigma^2}\right)\right)\quad (8)$$



Here,  $\mathbf{M}$  is the ground truth binary shadow mask computed after applying a fixed threshold on binary images.  $w_c$  is weight map to balance class frequencies,  $w_0$  and  $\sigma$  are hyper parameters.  $d_1$  and  $d_2$  are distances to the nearest and second nearest cell, respectively. We note from our experiments that this particular distance transform yields the most consistent convergence compared to other distance transforms, such as blurring.

**Shadow Mapping Loss.** We optimize our entire framework on binary shadow masks and train the MLP on the following loss:

$$\mathcal{L}_{sm} = \|w(\mathbf{M}, \sigma) - \hat{\mathbf{M}}\|^2 \quad (9)$$

Here,  $w(\mathbf{M}, \sigma)$  is the  $\sigma$  weighted ground truth shadow mask, and  $\hat{\mathbf{M}}$  is the predicted shadow mask from Equation (7).

## 4 Implementation

### 4.1 Dataset

We create a dataset of objects, including a cuboid, vase, chair and bunny, in blender. We render images of size  $800 \times 800$ . Although our approach does not have any constraints on the number or positions of light and camera, we fix the light source and randomly sample 200 camera positions on along the upper half of a sphere around the object. We include an ablation study regarding the number of shadow maps required for 3D reconstruction in the supplementary materials. For our approach, we only consider top down/satellite views with the light source being very far away from the camera and the object to represent a distant “sun-like” source. Our dataset motivates the use of shadows for 3D reconstruction because in overhead imagery, vertical surfaces, like facades, are sampled poorly, whereas oblique lighting can expose this geometry. We also open source our datasets to be used for future work, and provide links in the supplementary materials section.

### 4.2 Training

We use a faster implementation of NeRF [16] from [23], which uses PyTorch Lightning as its backend [22] [5]. We down sample all images from  $800 \times 800$  to  $64 \times 64$  to fit on one RTX-3080 GPU. We use the same positional encoding scheme,  $\gamma(x)$  and the MLP configuration  $f_\theta$  used in [16]. For camera projections, we write a custom *Planar Projection Camera* class that encapsulates the projections and readily works with OpenGL and blender cameras. We gradually decreases the  $\sigma$  hyperparameter in the distance transform (Equation 8) from  $\{150, 100, 50\}$  during training to encourage the network to learn coarse to fine geometry. We also train a Vanilla NeRF model on RGB images of the same scene on resolution  $64 \times 64$ . To reconstruct the meshes, we run marching cubes on the learned implicit representations. More information on the exact training details is given in the supplementary materials section, including details about our more efficient differentiable shadow mapping implementation, which decreases the training time by half.

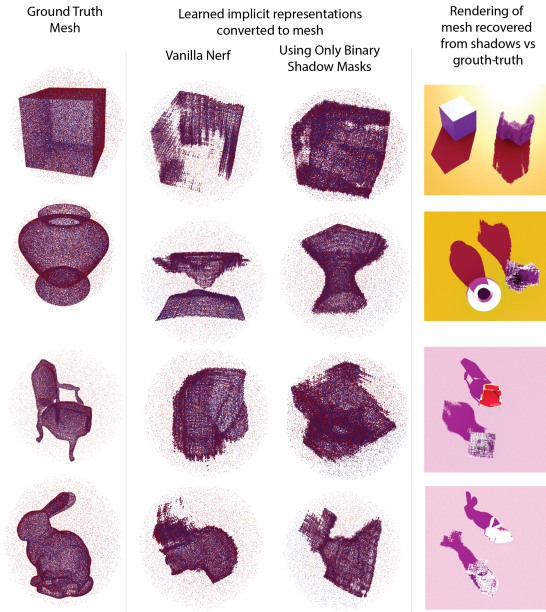


**Fig. 4. Qualitative Results.** We qualitatively compare mesh representations learned from a vanilla NeRF [16] trained on RGB images (column 2) and our proposed approach that uses *only* shadow masks (column 3) after running marching cubes [14]. We observe that for overhead views of the scene where the vertical surface of the vase is sampled poorly, vanilla NeRF fails to exploit hidden geometry cues in the cast shadows. Our approach is able to infer a better estimate and leverage the hidden cue just by using binary shadow masks. Even though the meshes are coarse, column 4 illustrates that their rendered shadows are very similar, indicating that the differentiable rendering framework can indeed learn from sparse shadow cues but, due to lack of imposed priors on the object, it infers a geometry that will minimize difference between the predicted and true shadow. Some parts of the objects such as the upper face of cuboid are never in shadow, therefore there is no reconstruction for those surfaces our approach.

## 5 Results

**Evaluation Details.** We evaluate the performance of our method using root mean square error (RMSE) between the predicted point cloud and the ground truth point cloud, acquired with the iterative closest point (ICP) [1] algorithm, as reported in Table 1. In addition, we assess the visual quality of the predicted depth and shadow masks, and surface mesh, as shown in Figures 4 and 5. The thresholds used to get the mesh from a volumetric representation are given in supplementary.

**3D Reconstruction Results.** We show the learned scene representations qualitatively by converting them to explicit meshes and rendering them using a signed distance function (SDF). Figure 4 shows the estimated meshes from our method

Scene	RMSE Shadow Mesh	RMSE Vanilla NeRF
Cuboid	<b>0.0078</b>	0.097
Vase	<b>0.010</b>	0.0.011
Bunny	0.0109	<b>0.0106</b>
Chair	<b>0.0092</b>	0.0096

**Table 1.** We quantitatively analyze the quality of the reconstructed meshes by running ICP [1] on meshes generated by our proposed method, which only uses binary shadows masks, and meshes generated by a vanilla NeRF trained on full RGB images. We show RGB images from Vanilla NeRF in the supplementary materials along with training details.

on four object types. We compare our meshes to meshes generated by vanilla NeRF run on RGB images, and the ground truth. Our datasets are rendered with overhead camera viewpoints, which enables shadows to be exploited. Given the binary nature of shadow masks and how little information shadows encode when compared to RGB images, we observe that our forward model coupled with the differentiable rendering framework finds good coarse estimates of the objects. Moreover, in the case of vases, the mesh reconstruction benefits from exploiting shadows as the algorithm can use *hidden* cues present in the scene, such as the curvature of the vase, which are not readily visible when relying on photometric cues. We also show predicted depth maps and shadow masks on novel camera viewpoints not used during training in the supplementary materials.

**Novel Viewpoint Rendering.** We observe predicted depth and shadow masks rendered from novel viewpoints in Figure 5. The depth maps converge quite quickly to localize the object even when optimizing on the sparse physical cue of shadows. We posit that this convergence shows how powerful differentiable rendering is for exploiting physical cues to enable better 3D reconstruction. The depth maps converge slowly and we nudge the convergence by gradually decreasing the sigma values for the distance transform. The use of the distance transform leads to blurrier boundaries, however, the rendered mesh shows that a reasonably coarse 3D estimate is captured.

**Quantitative Analysis.** We also run our datasets on a vanilla NeRF [16] implementation [23]. At lower resolutions and aerial imagery, we see that the NeRF approach fails to provide a reasonable fine mesh. We believe this failure is due to the down-sampling of images to  $64 \times 64$ , which may also be a reason as to why our meshes fail to capture fine details. We run ICP [1] on the generated points cloud and show on-par results to the NeRF approach. Our goal, however, is not to outperform NeRF but to show the effectiveness of differentiable rendering framework in exploiting physical cues instead of ignoring them. The main takeaway from Table 1 is that differentiable volumetric renderers do not need to rely on 8 bit RGB information to reconstruct accurate meshes, but can also leverage other sources of information in the image in addition to relying on photometric cues.

**Limitations.** In cases such as the cuboid and the vase, we observe that the renderer converges to a predicted mesh that minimizes the shadow masks and

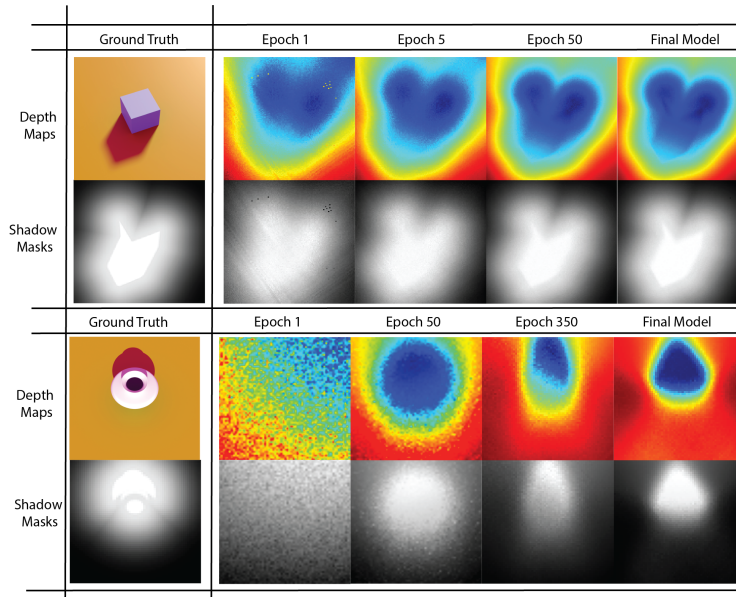


**Fig. 5. Evolution of depth maps during training through a novel camera viewpoint.** We visualize how the proposed forward model and differentiable rendering framework quickly converges to localize the object based on very sparse shadow cues present in the image and then slowly refines the coarse estimate on novel camera viewpoints. We believe that these results reveal that the differentiable volumetric rendering is a powerful framework that can learn critical information about the scene by relying and exploiting only sparse cues. We show predicted depth maps on other objects in the supplementary material.

the predicted shape even though it is typically a coarse estimate that envelopes the entirety of the object. This means that we see artifacts such as the pointed curve in the vase mesh, or the curvature of the bunny. In addition, we can also observe that the learned geometry is in-sync with the scene’s lighting direction and the available shadow information. Since our algorithm only has geometry information where the binary shadow mask is true, areas that are never in shadow have no surface, which leads to incomplete meshes. This phenomena is shown for the cuboid case in column 4 of Figure 4, where there is no estimated surface along the cuboid’s faces that are oriented towards the light, and can also be observed in the vase’s and chair’s case.

## 6 Discussions

**Exploiting Physical Cues.** One of the major goals of our work is to propose a framework within neural rendering that can readily exploit and learn from sparse physical cues, such as shadows, instead of ignoring them when doing 3D reconstruction from 2D images. We believe that Figure 5 shows that sparse

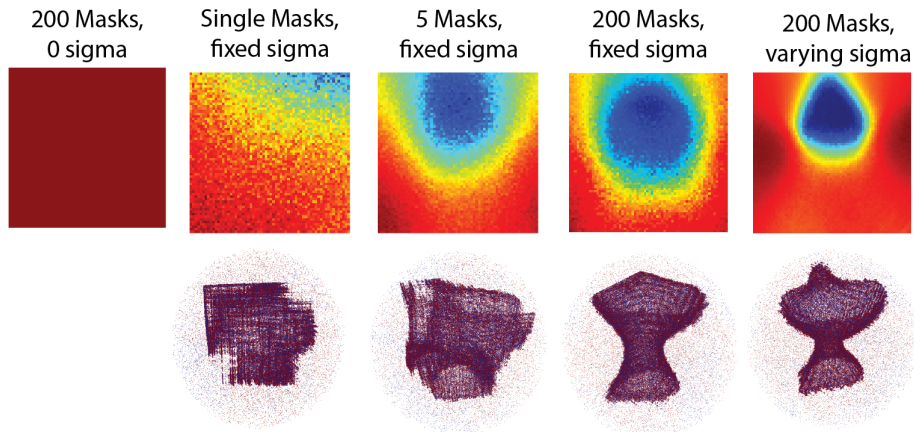


**Fig. 6. Ablation on sigma and number of shadow masks.** We study the importance of the distance transform in our method. Without the distance transform to guide and smooth-en the shadow masks, there is no convergence in the depth maps or the mesh. We notice an iterative coarse to fine mesh estimation done by the framework as we increase the number of masks and vary sigma. We observe that the number of masks carves the space down to create finer meshes. Varying sigma with many shadow masks yields the best results although it can overfit to the shadow mask and cause mesh artifacts. We discuss our ablations in more detail in the supplementary material.

physical cues like shadows, actually encode a lot of *hidden* information about the scene and can be used in isolation to reconstruct the underlying scene. By constructing explicit forward models that are readily differentiable and leveraging gradient-friendly volumetric rendering, we can exploit these cues in conjunction with relying on photometric consistency between images. Optimizing over photometric and a physical cue of shadows, for example, could lead to a better reconstruction in scenarios where there is uniform texture, low image resolution, or in cases of overhead imagery where vertical surfaces and facades are poorly sampled. We posit that modern data-driven 3D reconstruction techniques can benefit greatly from exploiting physical cues such as shadows, reflections, polarization etc., instead of only relying on photometric consistency.

**Differentiable Shadow Rendering.** Shadow mapping is very well suited for rasterization, and volumetric rendering is inherently a ray marching approach. Shadow mapping is extremely efficient as it requires the shadow map to be computed once. Moreover, shadows in ray tracing are expensive as every ray needs to compute a path to the light source to determine if it is in shadow, and, therefore, many ray tracing approaches also use shadow mapping to compute shadows efficiently and accurately in the scene. Our approach, like the traditional shadow mapping, assumes a binary label on shadows and does not consider soft shadows or ambient lighting. However, our goal is to exploit shadows to do 3D reconstruction, not to render photorealistic images, so an imprecise method to compute shadows (thresholds over RGB images) is sufficient. Although we

do not extend our framework to varying light sources, our approach is readily extendable to varying light and camera sources.

### 6.1 Future Work

We observe that volumetric rendering can converge onto coarse estimates of the object geometry by only relying on shadows, and applications, such as non-line-of-sight imaging (NLOS) [31] and imaging behind occluders [7], rely on shadows to reconstruct the occluded object. Moving towards a differentiable formulation to these problems can make them robust to real world scenes and complex hidden objects. Shadows themselves are never the only cue present to reconstruct the scene. Moreover, our framework is incredibly easy to integrate with existing NeRF approaches that rely only on photometric cues. Our shadow loss [7] can be used as a regularizer or an auxiliary loss to constrain the renderer, especially as shadows are invariant to viewpoint changes, surface reflectance properties, or texture changes. Additionally, we also hope to inspire future work in exploiting physics based cues in modern data-driven neural rendering techniques.

### 6.2 Conclusions

We show that neural scene representations can learn 3D geometry from just binary shadow masks. We are motivated by traditional shape-from-X algorithms that typically construct a physics driven inverse model that can exploit a physical cue to reconstruct the underlying 3D object. We observe that data-driven neural rendering frameworks ignore such physical cues, such as shadows, and instead rely heavily on photometric cues for scene reconstruction. We thus propose a graphics-inspired differentiable shadow rendering component that leverages a gradient-friendly volumetric renderer as its inverse model to learn geometry from shadows. We then train an implicit neural network to encode the scene. We observe that our method leads to coarse depth estimates sufficient for 3D reconstruction.

## References

1. Besl, P., McKay, N.D.: A method for registration of 3-d shapes. *IEEE Transactions on Pattern Analysis and Machine Intelligence* **14**(2), 239–256 (1992). <https://doi.org/10.1109/34.121791>
2. Bobrow, D.G.: Comment on “Numerical shape from shading and occluding boundaries”, pp. 89–94 (1994)
3. Boss, M., Braun, R., Jampani, V., Barron, J.T., Liu, C., Lensch, H.P.: NerD: Neural reflectance decomposition from image collections. In: *IEEE International Conference on Computer Vision (ICCV)* (2021)
4. Chang, A.X., Funkhouser, T., Guibas, L., Hanrahan, P., Huang, Q., Li, Z., Savarese, S., Savva, M., Song, S., Su, H., Xiao, J., Yi, L., Yu, F.: ShapeNet: An Information-Rich 3D Model Repository. Tech. Rep. arXiv:1512.03012 [cs.GR], Stanford University — Princeton University — Toyota Technological Institute at Chicago (2015)
5. Falcon et al., W.: Pytorch lightning. GitHub. Note: <https://github.com/PyTorchLightning/pytorch-lightning> **3** (2019)
6. Guo, Y., Kang, D., Bao, L., He, Y., Zhang, S.: Nerfren: Neural radiance fields with reflections. *CoRR* **abs/2111.15234** (2021), <https://arxiv.org/abs/2111.15234>
7. Henley, C., Maeda, T., Swedish, T., Raskar, R.: Imaging behind occluders using two-bounce light. In: Vedaldi, A., Bischof, H., Brox, T., Frahm, J.M. (eds.) *Computer Vision – ECCV 2020*. pp. 573–588. Springer International Publishing, Cham (2020)
8. Kato, H., Ushiku, Y., Harada, T.: Neural 3d mesh renderer. In: *The IEEE Conference on Computer Vision and Pattern Recognition (CVPR)* (2018)
9. Landabaso, J.L., Pardàs, M., Casas, J.R.: Shape from inconsistent silhouette. *Comput. Vis. Image Underst.* **112**, 210–224 (2008)
10. Li, T.M., Aittala, M., Durand, F., Lehtinen, J.: Differentiable monte carlo ray tracing through edge sampling. *ACM Trans. Graph. (Proc. SIGGRAPH Asia)* **37**(6), 222:1–222:11 (2018)
11. Liu, S., Li, T., Chen, W., Li, H.: Soft rasterizer: A differentiable renderer for image-based 3d reasoning. In: *Proceedings of the IEEE/CVF International Conference on Computer Vision*. pp. 7708–7717 (2019)
12. Lombardi, S., Simon, T., Saragih, J., Schwartz, G., Lehrmann, A., Sheikh, Y.: Neural volumes: Learning dynamic renderable volumes from images. *ACM Trans. Graph.* **38**(4), 65:1–65:14 (Jul 2019)
13. Loper, M.M., Black, M.J.: Opendr: An approximate differentiable renderer. In: *European Conference on Computer Vision*. pp. 154–169. Springer (2014)
14. Lorensen, W.E., Cline, H.E.: Marching cubes: A high resolution 3d surface construction algorithm. *ACM siggraph computer graphics* **21**(4), 163–169 (1987)
15. Martin, W.N., Aggarwal, J.K.: Volumetric descriptions of objects from multiple views. *IEEE Transactions on Pattern Analysis and Machine Intelligence* **PAMI-5**(2), 150–158 (1983). <https://doi.org/10.1109/TPAMI.1983.4767367>
16. Mildenhall, B., Srinivasan, P.P., Tancik, M., Barron, J.T., Ramamoorthi, R., Ng, R.: NeRF: Representing scenes as neural radiance fields for view synthesis. In: *The European Conference on Computer Vision (ECCV)* (2020)
17. Niemeyer, M., Geiger, A.: GIRAFFE: Representing scenes as compositional generative neural feature fields. <https://arxiv.org/abs/2011.12100> (2020)

18. Niemeyer, M., Mescheder, L., Oechsle, M., Geiger, A.: Differentiable volumetric rendering: Learning implicit 3D representations without 3D supervision. In: Proceedings of the IEEE/CVF Conference on Computer Vision and Pattern Recognition (CVPR) (2019)
19. Niemeyer, M., Mescheder, L., Oechsle, M., Geiger, A.: Differentiable volumetric rendering: Learning implicit 3d representations without 3d supervision. In: Proc. IEEE Conf. on Computer Vision and Pattern Recognition (CVPR) (2020)
20. Nimier-David, M., Vicini, D., Zeltner, T., Jakob, W.: Mitsuba 2: A retargetable forward and inverse renderer. *ACM Transactions on Graphics (TOG)* **38**(6), 1–17 (2019)
21. Park, J.J., Florence, P., Straub, J., Newcombe, R., Lovegrove, S.: DeepSDF: Learning continuous signed distance functions for shape representation. In: Proceedings of the IEEE/CVF Conference on Computer Vision and Pattern Recognition (CVPR). pp. 165–174 (2019)
22. Paszke, A., Gross, S., Massa, F., Lerer, A., Bradbury, J., Chanan, G., Killeen, T., Lin, Z., Gimelshein, N., Antiga, L., Desmaison, A., Kopf, A., Yang, E., DeVito, Z., Raison, M., Tejani, A., Chilamkurthy, S., Steiner, B., Fang, L., Bai, J., Chintala, S.: Pytorch: An imperative style, high-performance deep learning library. In: Wallach, H., Larochelle, H., Beygelzimer, A., d'Alché-Buc, F., Fox, E., Garnett, R. (eds.) *Advances in Neural Information Processing Systems 32*, pp. 8024–8035. Curran Associates, Inc. (2019), <http://papers.neurips.cc/paper/9015-pytorch-an-imperative-style-high-performance-deep-learning-library.pdf>
23. Quei-An, C.: Nerf.pl: a pytorch-lightning implementation of nerf (2020), [https://github.com/kwea123/nerf\\_pl/](https://github.com/kwea123/nerf_pl/)
24. Ronneberger, O., Fischer, P., Brox, T.: U-net: Convolutional networks for biomedical image segmentation (2015)
25. Sara Fridovich-Keil and Alex Yu, Tancik, M., Chen, Q., Recht, B., Kanazawa, A.: Plenoxels: Radiance fields without neural networks. In: CVPR (2022)
26. Savarese, S., Rushmeier, H., Bernardini, F., Perona, P.: Shadow carving. In: Proceedings Eighth IEEE International Conference on Computer Vision. ICCV 2001. vol. 1, pp. 190–197. IEEE (2001)
27. Sitzmann, V., Thies, J., Heide, F., Nießner, M., Wetzstein, G., Zollhofer, M.: Deepvoxels: Learning persistent 3d feature embeddings. In: Proceedings of the IEEE/CVF Conference on Computer Vision and Pattern Recognition. pp. 2437–2446 (2019)
28. Srinivasan, P.P., Deng, B., Zhang, X., Tancik, M., Mildenhall, B., Barron, J.T.: Nerv: Neural reflectance and visibility fields for relighting and view synthesis (2020)
29. Tancik, M., Srinivasan, P.P., Mildenhall, B., Fridovich-Keil, S., Raghavan, N., Singhal, U., Ramamoorthi, R., Barron, J.T., Ng, R.: Fourier features let networks learn high frequency functions in low dimensional domains (2020)
30. Tulsiani, S., Efros, A.A., Malik, J.: Multi-view consistency as supervisory signal for learning shape and pose prediction. In: Computer Vision and Pattern Recognition (CVPR) (2018)
31. Velten, A., Willwacher, T., Gupta, O., Veeraraghavan, A., Bawendi, M.G., Raskar, R.: Recovering three-dimensional shape around a corner using ultrafast time-of-flight imaging. *Nature* p. 745 (2012)
32. Verbin, D., Hedman, P., Mildenhall, B., Zickler, T., Barron, J.T., Srinivasan, P.P.: Ref-NeRF: Structured view-dependent appearance for neural radiance fields. arXiv (2021)



33. Vis, J., Yamazaki, S., Srinivasa, , Narasimhan, G., Baker, S., Kanade, T., Narasimhan, S.: The theory and practice of coplanar shadowgram imaging for acquiring visual hulls of intricate objects. *International Journal of Computer Vision* **81** (03 2009). <https://doi.org/10.1007/s11263-008-0170-4>
34. Vogel, O., Valgaerts, L., Breuß, M., Weickert, J.: Making shape from shading work for real-world images. In: Denzler, J., Notni, G., Süße, H. (eds.) *Pattern Recognition*. pp. 191–200. Springer Berlin Heidelberg, Berlin, Heidelberg (2009)
35. Williams, L.: Casting curved shadows on curved surfaces. In: *Proceedings of the 5th annual conference on Computer graphics and interactive techniques*. pp. 270–274 (1978)
36. Ye, Y., Tulsiani, S., Gupta, A.: Shelf-supervised mesh prediction in the wild. In: *Computer Vision and Pattern Recognition (CVPR)* (2021)
37. Yu, A., Li, R., Tancik, M., Li, H., Ng, R., Kanazawa, A.: PlenOctrees for real-time rendering of neural radiance fields. In: *ICCV* (2021)
38. Zhang, J.Y., Yang, G., Tulsiani, S., Ramanan, D.: NeRS: Neural reflectance surfaces for sparse-view 3d reconstruction in the wild. In: *Conference on Neural Information Processing Systems* (2021)
39. Zhang, R., Tsai, P.S., Cryer, J., Shah, M.: Shape-from-shading: a survey. *IEEE Transactions on Pattern Analysis and Machine Intelligence* **21**(8), 690–706 (1999). <https://doi.org/10.1109/34.784284>
40. Zheng, Q., Chellappa, R.: Estimation of illuminant direction, albedo, and shape from shading. *IEEE Transactions on Pattern Analysis and Machine Intelligence* **13**(7), 680–702 (1991). <https://doi.org/10.1109/34.85658>

# Supplementary Information

Kushagra Tiwary <sup>\*†</sup>, Tzofi Klinghoffer <sup>\*</sup>, and Ramesh Raskar

Massachusetts Institute of Technology  
{ktiwary, tzofi, raskar}@mit.edu

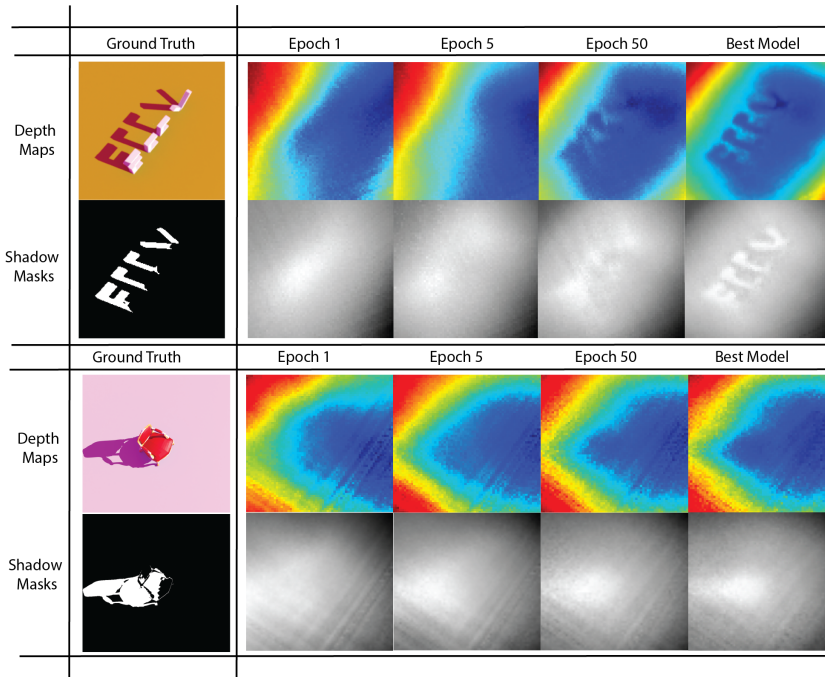


**Fig. S.1. Predicted depth maps and shadow masks for a scene with multiple objects and a chair during training on validation poses.** Reconstructing any 3D representation from the object’s binary shadow masks is a very hard and we show that we can extend our algorithms to a scene with **arbitrary** number of objects. This is due to our use of implicit volumetric representation and that our algorithm makes limited assumptions about the scene or its objects.

Reconstructing any 3D representation just from the object’s binary shadow masks is a very hard and unsolved problem. Shadows possess important geometric information about the object, however, due to the ill-posedness, many different kinds of objects that have similar appearance in 2D can cast the same shadow. Moreover, these objects can map to the same shadow mask and have very different underlying 3D shapes making this problem more difficult than recovering 3D geometry from images. Our algorithm makes limited assumptions about the underlying scene working with hard shadows. It also doesn’t assume

the number of objects in the scene and tries to fit the best 3D model that explains the shadows masks.

## S.1 Results

We show predicted depth and shadow masks on a scene with multiple objects and the chair in Figure S.1, and on a bunny object in Figure S.3. In the first row of Figure S.1, we run our method on a scene with multiple objects that spell **ECCV**. If we had used explicit meshes, we would have to specify the number of objects before training, however, by parametrizing the scene with opacities, we can scale up to an arbitrary number of objects placed in any position in the scene. For the scene with multiple objects, we generate shadows masks and feed them to the proposed algorithm as input, without specifying additional information. Since our algorithm does not assume any prior knowledge about the scene or its objects, it can optimize over and find the best volumetric densities that explain the shadow mask. This result further shows how traditional algorithms like shape-from-shadows/x can benefit from differentiable volumetric rendering as they can now scale to arbitrary number of objects and more complex scenes.

For the chair object in Figure S.1, observe how the chair is on the right of the casted shadows and the model accurately predicts and segments out that area, including able to infer the sharp corner.

As shown in Figure S.3, the model is able to learn the course shape and localize the bunny well through its shadow map. However, it fails to carve out the ears and the finer details. Our shape-from-shadow algorithm has the poorest performance on the bunny (Figure S.3), most likely due to its complexity, curved surfaces and its protruding ears that can imply many different possible combinations of the underlying 3D shape. Note that the model is trained on coarser versions of the fine shadow masks (shown in first column), similar to the training scheme described in Supplementary Section S.2.

## S.2 Implementation

**Model Details.** During training, we set  $\beta$   $1\mathbf{e}^{-2}$  or  $1\mathbf{e}^{-3}$  and  $\epsilon$  is usually set to 0. We set the  $\mu_{min}, \mu_{max}$  to be 0 and 1 respectively and compute gradients directly on the normalized values instead of using the sigmoid. For the position encoding we also use parameters from the original NeRF implementation. We use an 8-layer MLP to parametrize our scene. To enable better depth reconstruction we also use a coarse and a fine MLP, the coarse is sampled 64 times and the fine 128. Our MLP, however, does not have an extra head for the color and does not take the viewing direction as input.

**Training Scheme.** To train the model, we use the PyTorch implementation of the Adam optimizer [2], use a learning of  $5 \times 10^{-4}$  and use a step function to decay the learning rate at 20 epochs. We evaluate our model on the validation data, and test it against real meshes from blender. We start training with a high distance setting for our distance transform  $\sigma = \{100, 150\}$  and train for

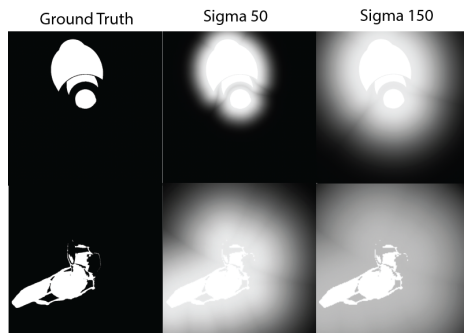


**Fig. S.2. Increasing the distance transform weight "sigma" hyperparameter.** We show the shadow maps that the model actually learns on. We apply the distance transform and slowly decrease it in our training. The transform helps with taking smoother gradients wrt the model's parameters.

150 epochs. Then we lower the  $\sigma = \{50, 45\}$  to continue training. We note that using a  $\sigma$  value lower than this causes our model to diverge and start to learn spurious depth maps. Our entire implementation trains on one Tesla V-100 and takes a half a day. The models were typically trained to run for 200/300 epochs where each epoch runs on all rays generated from all camera pixels. Only the cuboid was trained on 2 Tesla V100s on an image of size  $128 \times 128$  with 64 fine and coarse samples. This training took 3 days to complete.

**Efficient Differentiable Shadow Rendering.** Our approach requires two NeRF forward passes per epoch to train: one from the light's perspective and one from the camera. To make training faster, we implemented a more efficient method to compute depths. We exploited the fact that our method requires the shadow map array to be indexed by the projected camera pixels, therefore we only need to compute a full shadow map on  $H \times W$  rays and can batch the camera rays. This approach worked really well and decreased our computation budget by roughly half. Moreover, our method does not make any assumption on the size of the camera and light depth arrays, and therefore we could also use a smaller shadow map. We also implemented a more efficient method of projecting the camera pixels into the light frame of reference, first and only computing the light depths on the projected locations instead of computing the full shadow map. This implementation, however, does not lead to any convergence, indicating that the loss computed on out-of-shadow pixels is also important and gives valuable information that helps in carving away that space to refine the mesh.

We also experimented with changing the number of fine samples used to sample opacities for a given light ray, computing gradients on the light opacities every  $K$  steps, in addition to sampling light depths at varying intervals instead of every step. Albeit many such methods did speed up training, we decided to use a basic setup which samples the light and camera rays with 64 coarse and 128 fine samples every iteration, with gradients being computed at each step.

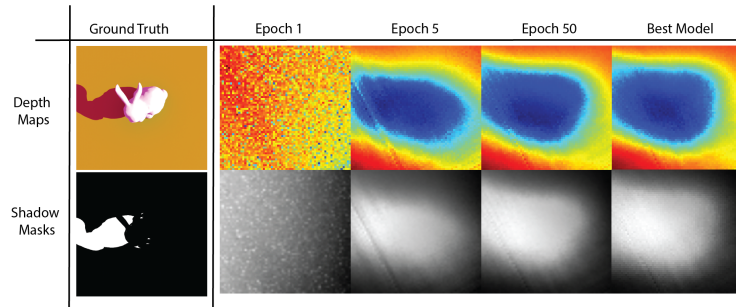


**Fig. S.3. Predicted depth maps and shadows masks during training on the bunny’s validation poses.** Even though the model is able to learn the greater shape and localize the bunny well through its shadow map, its poor performance is probably due to its complexity, curves surfaces and its protruding ears that can imply many different possible combinations of the underlying 3D shape.

**Explicit Mesh from Implicit Representations.** Extracting an explicit mesh from an implicit volumetric representation typically involves running marching cubes [4]. We used the PyMCubes library implementation of the marching cubes algorithm. To do this, we create a bounding volume around the object and query the 3D volume for opacities at points inside the cuboid. In practice, we query along each dimension 128 to 256 of the volume of size  $(H, W, D)$  therefore creating voxels of size  $H/128, W/128, D/128$ . We query for an opacity at every voxel once to create a volume that can then be fed into the marching cubes algorithm. We use a set contour value of 0 to search for isosurfaces in volume. This gives us a non-smooth mesh explicit mesh with vertices and triangular faces which is then used for visualization and evaluation. Note that the volume bounds are different for each object and we find them using trial and error. In  $(x, y, z)$  direction, they are  $\{\pm 5\}$  for cuboid,  $\{\pm 35\}$  for chair,  $\{\pm 45\}$  for vase and  $\{\pm 35\}$  bunny. We refer our readers to our code for more information. Additionally, we do want to note that extracting explicit meshes from implicit representations is an extremely difficult task which requires a lot of trial and error. Even when results look great for novel view synthesis with the RGB NeRF framework, marching cubes doesn’t produce perfect smooth meshes. Often these meshes have jagged edges and protruding elements. Moreover, this becomes a tremendous problem when there is more than one object, as we start to extract extremely noisy meshes. However, alignment of explicit meshes is one of the most accurate metrics for 3D reconstruction evaluation, which is why we use it as an evaluation metric.

**Weighted Shadow Masks.** We show examples of the weighted shadow masks that we actually train the model on in Figure S.2

**Code and Datasets.** Our code and datasets are available at this anonymous [google drive link](#)

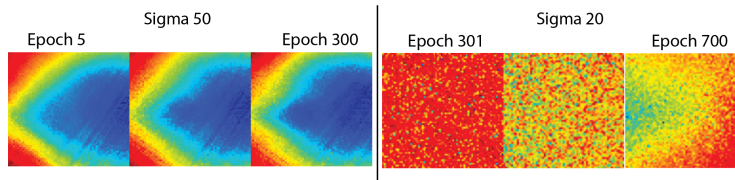


**Fig. S.4. Drastically changing distance transform weight during training for the Chair Object.** This figure shows the challenge in using shadows with a gradient based technique. Even though we reduce the weight during training, drastically reducing it can cause the model to unlearn the scene representation as the information it relied on converge to the object is now missing.

### S.3 Ablation Studies

We show in Figure 6 in the main text the final reconstructions from different experiments varying different parameters. We observe that starting from a smoothed-out shadow mask is critical for the algorithm to construct a coarse mesh and the algorithm almost never converges without smoothing applied to the initial binary shadow masks. This makes sense as the gradients are now non-zero around the edges of the binary mask, and can help guide the network in constructing a mesh that is consistent with all the shadow images. Smoothing techniques have also been used in [1] and [3] where the goal was to recover 3D mesh from a single silhouette image. Since the light is fixed in the scene and unchanged, the amount of information available about the object’s geometry is also fixed. The varying camera positions provide different viewpoints to the object and help the algorithm differentially carve away that space. We note that even with 5 shadow masks our algorithm is able to reconstruct a coarse object, however it isn’t able to carve away the right and the left parts of the vase which we believe is due to the lack of viewpoints from those poses. An oversampling of poses, we note that 200 views of the object means that some positions are sampled more than once, is more than enough to help the algorithm carve out the unnecessary elements in the mesh. We also show that varying the distance transform weight from 150 to 50, as shown in Figure 6 for the vase, can create crisper depth maps and faster convergence. However, this also leads to overfitting to the shadow mask since exactly fitting a mesh to the shadow doesn’t necessarily translate to inferring the actual underlying shape of the object due to fundamental ill-posedness of the problem.

In Figure S.4 we also show drastically reducing the distance transform weight from 50 to 20 can cause the model to unlearn the scene representation. This shows how little gradient information shadows contain and that the model needs to be consistently nudged in order for it to be guided to reconstruct the underlying mesh.